ISSN 0021-8944, Journal of Applied Mechanics and Technical Physics, 2016, Vol. 57, No. 4, pp. 690–700. © Pleiades Publishing, Ltd., 2016.
Original Russian Text © K. Asemi, H. Ashrafi, M. Shariyat.

THREE-DIMENSIONAL STRESS AND FREE VIBRATION ANALYSES OF FUNCTIONALLY GRADED PLATES WITH CIRCULAR HOLES BY THE USE OF THE GRADED FINITE ELEMENT METHOD

K. Asemi[a], H. Ashrafi[b], and M. Shariyat[c]

UDC 539.3

Abstract: Static and free vibration analyses of plates with circular holes are performed based on the three-dimensional theory of elasticity. The plates are made of a functionally graded material (FGM), and the volume fractions of the constituent materials vary continuously across the plate. The effective properties of the FGM plate are estimated by using the Mori–Tanaka homogenization method. A graded finite element method based on the Rayleigh–Ritz energy formulation is used to solve the problem. Effects of different volume fractions of the materials and hole sizes on the behavior of FGM plates under uniaxial tension are investigated. Natural frequencies of a fully clamped FGM plate with a circular cutout are derived. The results obtained are compared with available experimental data.

Keywords: three-dimensional elasticity theory, graded finite element method, functionally graded material, Rayleigh–Ritz energy formulation, free vibration.

DOI: 10.1134/S0021894416040131

INTRODUCTION

Functionally graded materials (FGMs) are a new generation of advanced composite materials wherein the volume fractions of the constituent materials vary continuously through the structure at the macroscopic level. Some advantages of the FGMs over laminated composites are elimination of the delamination mode of failure and reduction of thermal stresses, residual stresses, and stress concentration factors at interfaces [1]. The main disadvantage of laminated composites is the weakness of the interfaces between the adjacent layers known as a delamination phenomenon that may lead to a failure. Also, debonding between the matrix and fiber may cause high thermal stresses.

Owing to their high strength, FGM plates are widely used in different structures; thus, it is important to study the stresses and free vibrations of FGM plates under mechanical loads to optimize their resistance to failure.

Mechanical properties of FGM plates usually vary through the plate thickness in a continuous manner. Many researchers have recently attempted to study the bending behavior of FGM plates based on three-dimensional elasticity solutions [2–6]. Unfortunately, analytical methods can only be successfully applied to the structural analysis of FGMs with very simple geometrical and loading conditions, and numerical methods are needed in general cases. Finite element (FE) methods have become the most powerful and reliable tools for analyzing FGM structures during recent years. Finite element methods based on the first-order and third-order shear deformation plate theories were developed by Reddy and his colleagues [7, 8]. The majority of research activities aimed at the

[a]Islamic Azad University, Tehran, North Branch, Tehran, Iran; kamiran64@yahoo.com. [b]University of Kashan, Kashan, Iran; hashrafi@kashanu.ac.ir. [c]K. N. Toosi University of Technology, Tehran, Iran; m_shariya@yahoo.com; shariya@kntu.ac.ir. Translated from Prikladnaya Mekhanika i Tekhnicheskaya Fizika, Vol. 57, No. 4, pp. 136–148, July–August, 2016. Original article submitted February 26, 2014; revision submitted August 31, 2014.

 0021-8944/16/5704-0690 © 2016 by Pleiades Publishing, Ltd.

analysis of FGM plates are based on the theories of plates [9–16]. Santare and Lambros [17] and then Kim and Paulino [18] adopted a graded isoparametric FE approach for comparing the behaviors of graded versus conventional homogeneous elements under various loading conditions.

Some works can be found in the literature on modeling of nonhomogeneous structures by using the graded FE method [19–26]. It was shown in those studies that the conventional FE formulations lead to a discontinuous stress field in the direction perpendicular to the material property gradation, while the graded elements ensure a continuous and smooth variation. However, if the loading is parallel to the material gradation direction, the graded FE formulation leads to solutions with sharp jumps in the stress field at the element boundaries, whereas the conventional homogeneous FE formulation provides a continuous stress field. The use of graded finite elements has several benefits over the use of conventional homogeneous elements in the dynamic and wave propagation analyses.

In conventional FE methods, the boundaries of homogenous elements of a nonhomogeneous material act as discrete interfaces for the stress waves. These boundaries cause artificial wave reflections and have a cumulative effect on the magnitude and speed of propagating stress waves. Therefore, by using the graded FE method, in which the material property is graded continuously through the elements, the accuracy can be improved without refining the mesh size.

The presence of a cutout (hole) in a stressed plate creates highly localized stresses in the vicinity of this cutout. The stress analysis of an FGM plate having a hole and made of a homogeneous or orthotropic material under uniaxial tension was performed in [27–30]. Kubair and Bhanu-Chandar [31] investigated the effect of the material property nonhomogeneity on the stress concentration factor (SCF) due to a circular hole in an FGM panel by using a multiple isoparametric FE formulation. Mohammadi et al. [32] studied the stress concentration factor around a circular hole in an infinite FGM plate subjected to uniform biaxial tension and pure shear.

Hu et al. [33] used the theory of elastodynamics and employed the image method to investigate the multiple scattering and dynamic stress in a semi-infinite FGM slab with a circular cavity. Fang et al. [34] studied the multiple scattering and strain energy density in semi-infinite FGMs with a circular cavity by using the theory of multiple scattering of elastic waves and expansion of wave functions. Nath et al. [35] extended the finite difference technique to obtain the stress as well as the displacement components of the deformed shape of a boron/epoxy orthotropic composite plate with an internal hole subjected to a uniform tension at its two opposite ends. Janghorban and Zare [36] investigated the thermal effects on free vibrations of functionally graded nonuniform straight-sided plates with circular and non-circular cutouts by using the FE method. Using the theory of complex variable functions, Yang et al. [37] studied the two-dimensional stress distribution in an FGM plate with a circular hole (the material properties varied continuously along the radius and the FGM plate was modeled by the method of piecewise homogeneous layers) under arbitrary constant loads. Linkov and Rybarska-Rusinek [38] presented and compared two (exact and approximate) efficient methods to evaluate the stress concentration in multi-wedge systems with FGM wedges. In the above-mentioned studies, the two-dimensional stress distribution of an FGM plate with a circular hole was investigated.

The challenge of the present study is the static and free vibration analyses of FGM plates with a circular hole, based on the three-dimensional theory of elasticity. By using the three-dimensional graded FE method, the effects of variations of the volume fractions and hole sizes on displacement and stress fields are investigated, and the natural frequencies are obtained.

1. GOVERNING EQUATIONS

The governing equations of the problem are developed through the following sections.

1.1. Material Gradient and Geometry

Let us consider a rectangular FGM plate of length a, width b, and thickness h, so that $0 < x \leqslant a$, $0 < y \leqslant b$, and $0 < z \leqslant h$ (Fig. 1). The plate has a central hole of diameter d and is subjected to uniform tension in the x direction at the edges $x = 0$ and $x = L$, while other boundaries of the plate are free (x, y, and z are the axes of the Cartesian coordinate system).

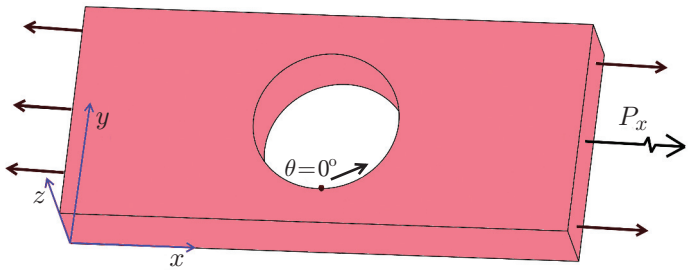

Fig. 1. Geometry of the FGM plate.

We assume that the FGM plate is made of two randomly distributed isotropic materials, and its properties vary only in the thickness direction. The volume fractions of the ceramic and metal phases are given by the formula

$$V_c = 1 - (z/h)^n, \qquad V_m = 1 - V_c,$$

where n is the non-negative volume fraction exponent; the subscripts c and m are used to denote the ceramic and metal materials, respectively.

The Mori–Tanaka homogenization method is used to find the effective properties at any arbitrary point. According to the Mori-Tanaka homogenization method, the effective bulk modulus K and the effective shear modulus G of the FGM plate may be found by the formulas

$$\frac{K - K_c}{K_m - K_c} = \frac{V_m}{1 + (1 - V_m)(K_m - K_c)/(K_c + 4G_c/3)}; \tag{1}$$

$$\frac{G - G_c}{G_m - G_c} = \frac{V_m}{1 + (1 - V_m)(G_m - G_c)/(G_c + f_c)}, \tag{2}$$

where

$$f_c = \frac{G_c(9K_c + 8G_c)}{6(K_c + 2G_c)}. \tag{3}$$

The effective values of the modulus of elasticity and Poisson's ratio are

$$E = \frac{9KG}{3K + G}, \qquad \nu = \frac{3K - 2G}{2(3K + G)}.$$

According to distributions (1)–(3), the bottom surface of the FGM plate is purely ceramic, the top surface is purely metallic, and different volume fractions of the constituents can be obtained for different values of n. The effective mass density of the FGM plate is determined by the rule of mixtures.

1.2. Equations of Motion

In the absence of body forces, the equations of motion for a rectangular FGM plate can be written as

$$\sigma_{ij,j} = \rho(z)\ddot{u}_i,$$

where i and j correspond to the x, y, and z coordinates, the comma denotes partial differentiation with respect to the Cartesian coordinate variables, and ρ is the mass density which depends on the z coordinate.

1.3. Stress–Strain Relations

In accordance with Hooke's law, the stress–strain relations of linear elasticity are written in the matrix form [39] as

$$[\sigma_{ij}] = \boldsymbol{D}\,[\varepsilon_{ij}],$$

where

$$\boldsymbol{D} = \frac{E(z)(1-\nu)}{(1+\nu)(1-2\nu)} \begin{pmatrix} 1 & \frac{\nu}{1-\nu} & \frac{\nu}{1-\nu} & 0 & 0 & 0 \\ \frac{\nu}{1-\nu} & 1 & \frac{\nu}{1-\nu} & 0 & 0 & 0 \\ \frac{\nu}{1-\nu} & \frac{\nu}{1-\nu} & 1 & 0 & 0 & 0 \\ 0 & 0 & 0 & \frac{1-2\nu}{2(1-\nu)} & 0 & 0 \\ 0 & 0 & 0 & 0 & \frac{1-2\nu}{2(1-\nu)} & 0 \\ 0 & 0 & 0 & 0 & 0 & \frac{1-2\nu}{2(1-\nu)} \end{pmatrix}. \tag{4}$$

It should be noted that Young's modulus E varies in the z direction and Poisson's ratio ν is assumed to be constant.

1.4. Strain–Displacement Relations

The strain–displacement relations of the infinitesimal theory of elasticity are presented in the following matrix form:

$$[\varepsilon] = [d][q], \qquad [d] = \begin{pmatrix} \partial/\partial x & 0 & 0 \\ 0 & \partial/\partial y & 0 \\ 0 & 0 & \partial/\partial z \\ (1/2)\,\partial/\partial y & (1/2)\,\partial/\partial x & 0 \\ 0 & (1/2)\,\partial/\partial z & (1/2)\,\partial/\partial y \\ (1/2)\,\partial/\partial z & 0 & (1/2)\,\partial/\partial x \end{pmatrix}, \qquad [q] = \begin{bmatrix} u \\ v \\ w \end{bmatrix}. \tag{5}$$

For an all-round clamped plate, the boundary conditions are

$$u(x,y,z)\Big|_{\substack{y=0\\y=b}} = 0, \qquad v(x,y,z)\Big|_{\substack{y=0\\y=b}} = 0, \qquad w(x,y,z)\Big|_{\substack{y=0\\y=b}} = 0,$$

$$u(x,y,z)\Big|_{\substack{x=0\\x=a}} = 0, \qquad v(x,y,z)\Big|_{\substack{x=0\\x=a}} = 0, \qquad w(x,y,z)\Big|_{\substack{x=0\\x=a}} = 0.$$

2. GRADED FINITE ELEMENT MODELING

Let us consider a three-dimensional 8-node linear brick element. In contrast to the conventional solid (brick) elements, the material properties are among the nodal degrees of freedom. Following the common FE approximation, the components of the displacement vector q of an arbitrary point of the element can be related to the nodal displacement vectors of the element through the shape function matrix N as

$$\boldsymbol{q}(\xi,\eta,\zeta) = \boldsymbol{N}(\xi,\eta,\zeta)\boldsymbol{\delta}^{(e)}, \tag{6}$$

where

$$\boldsymbol{\delta}^{(e)} = \{U_1, V_1, W_1, \ldots, U_8, V_8, W_8\}^{\mathrm{t}},$$

$$\boldsymbol{N}(\xi,\eta,\zeta) = \begin{bmatrix} N_1\ 0\ 0\ N_2\ 0\ 0\ N_3\ 0\ 0\ N_4\ 0\ 0\ N_5\ 0\ 0\ N_6\ 0\ 0\ N_7\ 0\ 0\ N_8\ 0\ 0 \\ 0\ N_1\ 0\ 0\ N_2\ 0\ 0\ N_3\ 0\ 0\ N_4\ 0\ 0\ N_5\ 0\ 0\ N_6\ 0\ 0\ N_7\ 0\ 0\ N_8\ 0 \\ 0\ 0\ N_1\ 0\ 0\ N_2\ 0\ 0\ N_3\ 0\ 0\ N_4\ 0\ 0\ N_5\ 0\ 0\ N_6\ 0\ 0\ N_7\ 0\ 0\ N_8 \end{bmatrix}.$$

The components of the shape function matrix can be expressed in terms of the local coordinates as [40, 41]

$$N_i(\xi,\eta,\zeta) = (1/8)(1+\xi_i\xi)(1+\eta_i\eta)(1+\zeta_i\zeta),$$

where $-1 \leqslant \xi \leqslant 1$, $-1 \leqslant \eta \leqslant 1$, and $-1 \leqslant \zeta \leqslant 1$. By using the graded FE method, the FGM material properties can also be determined based on their nodal values. Thus, the expressions for the modulus of elasticity E_i and mass density ρ_i corresponding to the ith node take the form

$$E(\zeta) = \sum_{i=1}^{8} E_i N_i(\xi,\eta,\zeta) = \boldsymbol{N\Xi}, \qquad \rho(\zeta) = \sum_{i=1}^{8} \rho_i N_i(\xi,\eta,\zeta) = \boldsymbol{N\Theta},$$

where $\boldsymbol{\Xi}$ and $\boldsymbol{\Theta}$ are the vectors of the nodal elasticity modulus and mass density, respectively:

$$\boldsymbol{\Xi} = (E_1, E_2, \ldots, E_8)^{\mathrm{t}}, \quad \boldsymbol{\Theta} = (\rho_1, \rho_2, \ldots, \rho_8)^{\mathrm{t}}, \quad \boldsymbol{N} = (N_1, N_2, \ldots, N_8)^{\mathrm{t}}.$$

Therefore, Eq. (4) can be rewritten as

$$\boldsymbol{D} = \boldsymbol{\Lambda N\Xi} = \boldsymbol{\Omega\Xi}.$$

Substitution of Eq. (6) into Eq. (5) yields the strain matrix of the element e:

$$\boldsymbol{\varepsilon}^{(e)} = \boldsymbol{dN}^{(e)}\boldsymbol{\delta}^{(e)} = \boldsymbol{B\delta}^{(e)}.$$

The governing equations of the FE model can be derived based on principle of the minimum total potential energy and the Rayleigh–Ritz method. The total potential energy of the plate can be expressed as

$$\begin{aligned}\Pi^{(e)} &= \frac{1}{2}\int\limits_{V^{(e)}} (\boldsymbol{\varepsilon}^{(e)})^{\mathrm{t}}\boldsymbol{\sigma}^{(e)}\,dV - \int\limits_{A^{(e)}} (\boldsymbol{q})^{\mathrm{t}}\boldsymbol{p}\,dA + \int\limits_{V^{(e)}} \rho(\boldsymbol{q})^{\mathrm{t}}\ddot{\boldsymbol{q}}^{(e)}\,dV \\ &= \frac{1}{2}\int\limits_{V^{(e)}} (\boldsymbol{\delta}^{(e)})^{\mathrm{t}}\boldsymbol{B}^{\mathrm{t}}\boldsymbol{\Omega\Xi B\delta}^{(e)}\,dV - \int\limits_{A^{(e)}} (\boldsymbol{\delta}^{(e)})^{\mathrm{t}}\boldsymbol{N}^{\mathrm{t}}\boldsymbol{p}\,dA \\ &\quad + \int\limits_{V^{(e)}} (\boldsymbol{\delta}^{(e)})^{\mathrm{t}}\boldsymbol{N}^{\mathrm{t}}\boldsymbol{N\Theta N}\ddot{\boldsymbol{\delta}}^{(e)}\,dV, \end{aligned} \tag{7}$$

where $V^{(e)}$ and $A^{(e)}$ are the volume and area of the element, $\boldsymbol{p}$ is the traction vector, and the last term of Eq. (7) represents the work of the inertial loads.

Therefore, employing the principle of the minimum total potential energy

$$\frac{\partial\Pi^{(e)}}{\partial\,(\boldsymbol{\delta}^{(e)})^{\mathrm{t}}} = 0$$

yields the following result:

$$\Big(\int\limits_{V^{(e)}} \boldsymbol{N}^{\mathrm{t}}\boldsymbol{N\Theta N}\,dV\Big)\ddot{\boldsymbol{\delta}}^{(e)} + \Big(\int\limits_{V^{(e)}} \boldsymbol{B}^{\mathrm{t}}\boldsymbol{\Omega\Xi B}\,dV\Big)\boldsymbol{\delta}^{(e)} = \int\limits_{A^{(e)}} \boldsymbol{N}^{\mathrm{t}}\boldsymbol{p}\,dA$$

or

$$\boldsymbol{M}^{(e)}\ddot{\boldsymbol{\delta}}^{(e)} + \boldsymbol{K}^{(e)}\boldsymbol{\delta}^{(e)} = \boldsymbol{F}^{(e)},$$

where

$$\boldsymbol{K}^{(e)} = \int\limits_{V^{(e)}} \boldsymbol{B}^{\mathrm{t}}\boldsymbol{\Omega\Xi B}\,dV, \quad \boldsymbol{M}^{(e)} = \int\limits_{V^{(e)}} \boldsymbol{N}^{\mathrm{t}}\boldsymbol{N\Theta N}\,dV, \quad \boldsymbol{F}^{(e)} = \int\limits_{A^{(e)}} \boldsymbol{N}^{\mathrm{t}}\boldsymbol{p}\,dA,$$

$$\boldsymbol{p} = (p_x, 0, 0)^{\mathrm{t}}.$$

As the plate is subjected to uniaxial tension along the x direction, the components of the traction vector are equal to zero in the y and z directions. The integrals of the mass and stiffness matrices are evaluated numerically by using eight Gaussian points and the Gauss–Legendre technique [41].

After assembling the element matrices, the global dynamic equilibrium equations for the FGM plate can be written as follows [41]:

$$[M]\{\ddot{\delta}\} + [K]\{\delta\} = 0.$$

For the static analysis, the governing equation reduces to

$$[K]\{\delta\} = \{F\}.$$

For the free vibration analysis, the problem reduces to the eigenvalue problem

$$([K] - [M]\omega^2)\{\delta\} = 0.$$

It should be noted that the problem may generally be solved in a rectangular Cartesian coordinates system followed by a transformation of the displacements and stresses into a polar coordinate system.

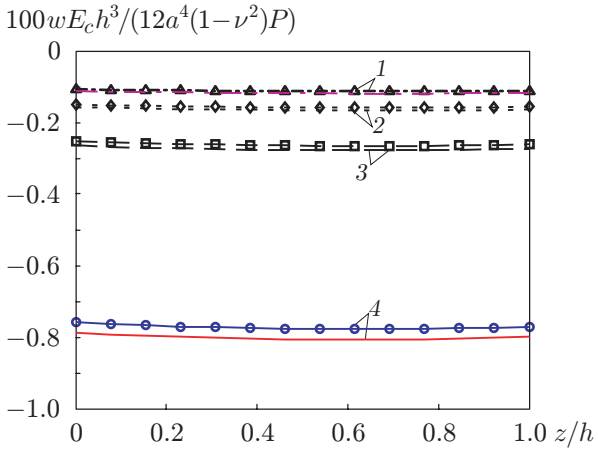

Fig. 2.

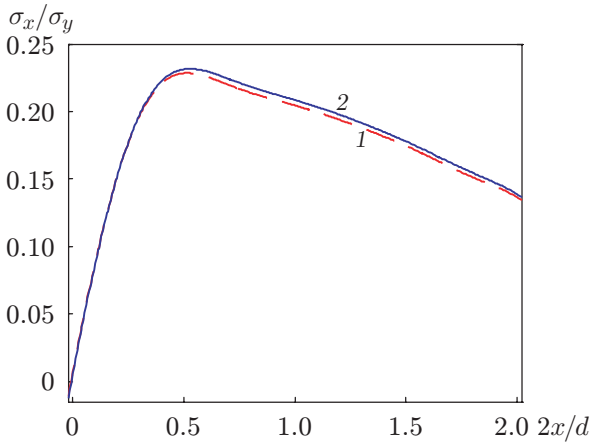

Fig. 3.

Fig. 2. Dimensionless displacements over the plate thickness h for $x = y = a/2$: the points and curves show the present results and the data of [42], respectively, for an all-round clamped plate (*1*), a plate with two simply supported and two clamped edges (*2*), a simply supported plate (*3*), and a plate with two simply supported and two free edges (*4*).

Fig. 3. Distributions of the in-plane stress ratio in front of the notch root versus the dimensionless coordinate for $z = h/2$ and $h/d = 1$ obtained in this work (*1*) and in [43] (*2*).

3. RESULTS AND DISCUSSION

The present section contains the results of the stress and free vibration analyses of the FGM plate.

3.1. Static Analysis

The written three-dimensional graded FE computer code for analyzing FGM plates with circular cutouts is verified by using data of an FGM plate with no hole under the same loading, which were previously reported in [42]. The plate is subjected to a uniform pressure at its upper surface. The problem parameters are $n = 1$, $a = b$, $h/a = 0.2$, $E_c = 70$ GPa, $E_m = 200$ GPa, $P = 1$ Pa, and $\nu = 0.3$.

The transverse distributions of dimensionless displacements across the FGM plate, which were obtained in the present work for different boundary conditions, are compared in Fig. 2 with those obtained in [42]. It is seen that the results are in good agreement.

To show the validity of the present solution for plates with a circular cutout, a homogenous plate [43] is considered. The plate is subjected to uniaxial tension. The problem parameters are $d = 2$ mm, $a = b = 200$ mm, $H = 2$ mm, and $E = 200$ GPa. The longitudinal distribution of the in-plane stress ratio σ_x/σ_y in front of the notch root as a function of the dimensionless coordinate $2x/d$ at $z = h/2$ is compared in Fig. 3 with the corresponding results of [43]. The results are seen to be in good agreement.

Let us consider a square FGM plate with a central hole having the diameter $d = 0.2$, 0.3, or 0.4 m, side length $a = b = 1$ m, and dimensionless thickness $h/a = 0.2$. The plate is made of a combined ceramic–metal material with $E_c = 380$ GPa, $\rho_c = 3800$ kg/m^3, $\rho_m = 2707$ kg/m^3, and $E_m = 70$ GPa. The plate is subjected to uniform tension in the x direction at the edges $x = 0$ and $x = L$, while its other boundaries are free. The static pressure and Poisson's ratio are taken as constant values: $P = 40$ MPa and $\nu = 0.3$. The number of graded elements in the z direction is 12 according to a mesh sensitivity study to ensure that the results converge reliably. Figure 4 shows the transverse distributions of the hoop stress across the plate. It is seen that the graded FE method provides a smoother and more accurate stress field than the conventional FE method for the same number of elements.

The transverse and circumferential distributions of the hoop stress for $\theta = 0°$ and around the hole at $z = h/2$ for $d = 0.4$ m and different values of the exponent n are shown in Figs. 5 and 6, respectively. Figure 5 shows that the transverse distribution of the hoop stress changes considerably with the exponent n. Figure 6 also illustrates

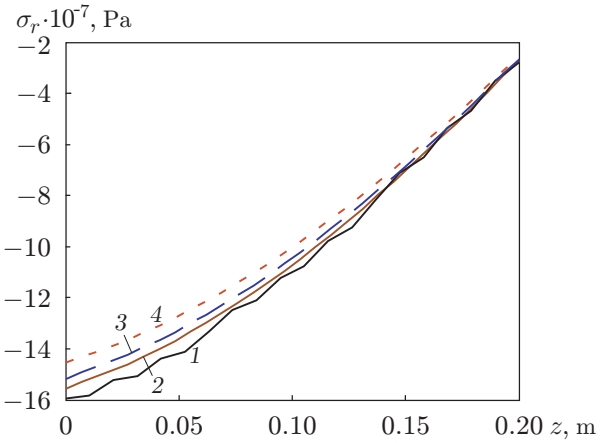

Fig. 4. Hoop stress distributions across the plate for $\theta = 0°$, $n = 1$, $d = 0.4$ m, and different numbers of graded finite elements (*1*, *3*, and *4*) and homogeneous finite elements (*2*): $ne_z = 12$ (*1* and *2*), 10 (*3*), and 8 (*4*).

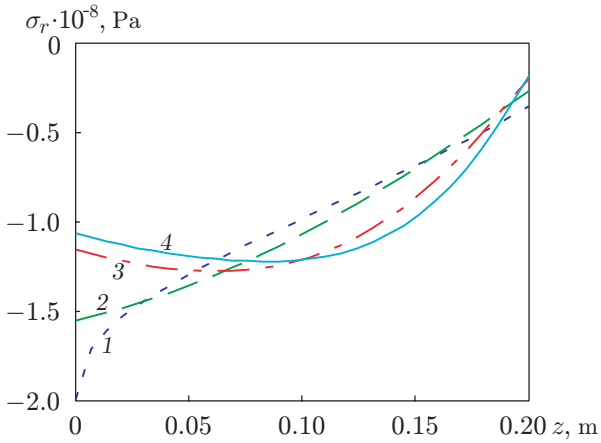

Fig. 5.

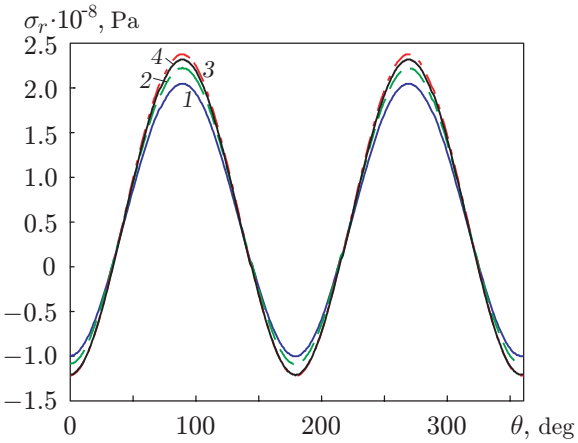

Fig. 6.

Fig. 5. Transverse distributions of the hoop stress for $\theta = 0°$, $d = 0.4$ m, and different values of n: $n = 0.5$ (*1*), 1 (*2*), 3 (*3*), and 5 (*4*).

Fig. 6. Circumferential distributions of the hoop stress for $z = h/2$, $d = 0.4$ m, and $n = 0.5$ (*1*), 1 (*2*), 3 (*3*), and 5 (*4*).

that the hoop stress around the hole increases for $n = 0.5$–3.0. The distributions of the hoop and axial stresses over the plate thickness for $\theta = 0°$, $n = 3$, and different hole diameters are shown in Fig. 7. It is seen that the hoop stress increases with increasing hole diameter, whereas the axial stress decreases. The results obtained show that the natural boundary conditions on the top and bottom surfaces of the FGM plate are satisfied, and the stress fields are continuous owing to the use of graded finite elements.

Figure 8 shows the transverse distributions of the radial displacement component for $\theta = 0°$, $d = 0.4$ m, and different values of the exponent n. In addition, the circumferential distributions of the hoop displacement component as a function of the coordinate θ are illustrated in Fig. 9 for $z = h/2$, $d = 0.4$ m, and different values of n. It is seen in Figs. 8 and 9 that the displacement fields decrease with increasing n. This behavior is caused by an increase in the modulus of elasticity due to increasing volume fraction of the ceramic phase. On the other hand,

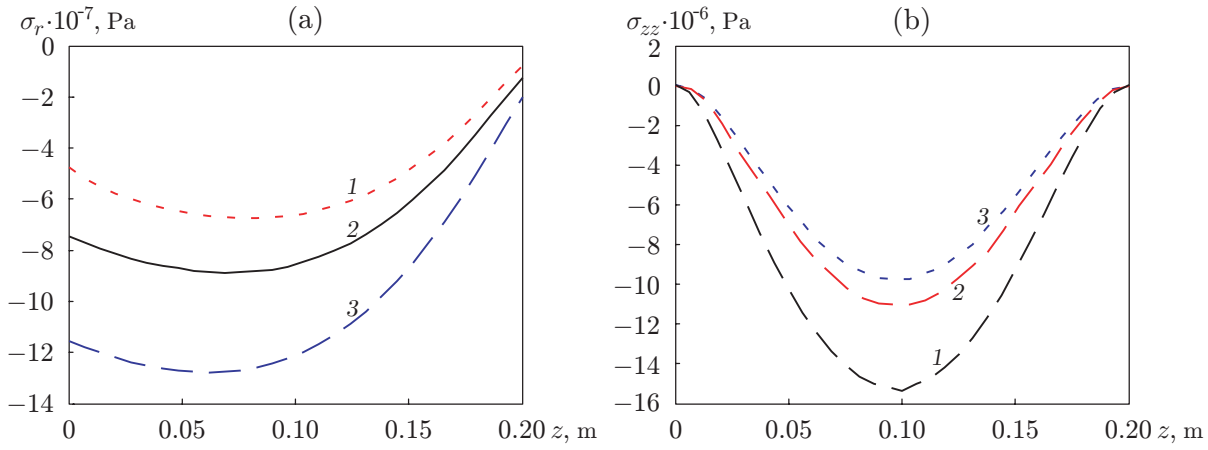

Fig. 7. Transverse distributions of the hoop (a) and axial (b) stresses for $\theta = 0°$, $n = 3$, and $d = 0.2$ (*1*), 0.3 (*2*), and 0.4 m (*3*).

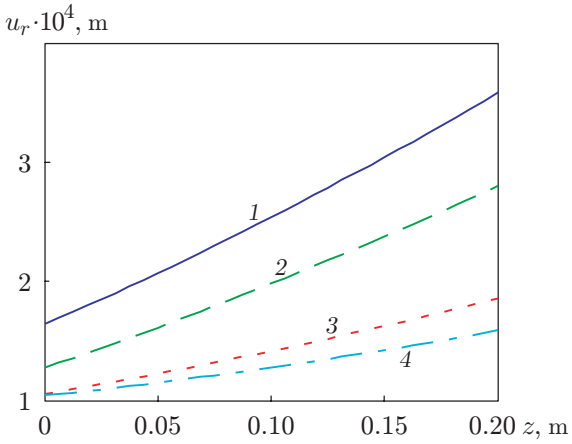

Fig. 8.

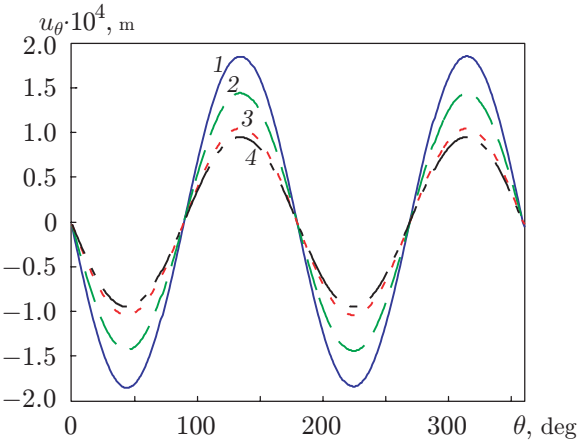

Fig. 9.

Fig. 8. Transverse distributions of the radial displacements for $\theta = 0°$, $d = 0.4$ m, and $n = 0.5$ (*1*), 1 (*2*), 3 (*3*), and 5 (*4*).

Fig. 9. Circumferential distributions of the hoop displacements for $z = h/2$, $d = 0.4$ m, and $n = 0.5$ (*1*), 1 (*2*), 3 (*3*), and 5 (*4*).

due to an asymmetric distribution of material properties, the stiffness of the lower layers becomes higher for larger values of n. For this reason, the radial displacements of various points across the plate are not identical. Therefore, the deformed shape of the initial cylindrical hole in the plate becomes a truncated cone with a noncircular base.

3.2. Free Vibration Analysis

We computed the natural frequencies for an FGM plate made of a combined ceramic–metallic material and compared them with the relevant analytical results for an FGM plate made of this material reported in [44]. The specifications of this plate are $a = b$, $h/a = 0.2$, $E_c = 70$ GPa, $E_m = 200$ GPa, $\rho_c = 2702$ kg/m^3, $\rho_m = 5700 = 5700$ kg/m^3, and $\nu = 0.3$. The dimensionless fundamental natural frequencies ($\bar{\omega} = \omega h\sqrt{\rho_c/E_c}$) for the clamped FGM plate calculated by the above-described algorithm and those reported in [43] are listed in Table 1, which shows good agreement between these results.

Table 1. Dimensionless fundamental natural frequencies $\bar{\omega}$ of a clamped FGM plate for different values of n

n	$\bar{\omega}$	
	Present work	Data of [44]
1	0.3231	0.3204
2	0.3197	0.3165
5	0.3181	0.3154

Table 2. Natural frequencies of a clamped FGM plate for different values of n and d

Mode number	ω, Hz								
	$d = 0.2$ m			$d = 0.3$ m			$d = 0.4$ m		
	$n = 0.5$	$n = 1.0$	$n = 5.0$	$n = 0.5$	$n = 1.0$	$n = 5.0$	$n = 0.5$	$n = 1.0$	$n = 5.0$
1	1907.8	2066.8	2381.1	2039.6	2209.5	2546.9	2293.2	2486.3	2868.7
2	3111.1	3398.9	3924.0	2971.5	3243.0	3744.7	2946.9	3211.6	3709.8
3	3111.9	3399.8	3925.0	2973.5	3245.3	3747.4	2947.5	3212.2	3710.5
4	4304.9	4713.0	5449.3	4221.5	4621.2	5339.8	4076.6	4459.5	5151.1
5	4709.3	5202.8	5996.3	4785.6	5249.3	6069.5	4578.6	5017.4	5802.4
6	4709.4	5202.9	5996.3	4997.7	5525.8	6394.7	5384.3	5955.1	6922.2
7	4898.0	5372.9	6217.6	4998.1	5526.2	6395.0	5384.4	5955.2	6922.2
8	5218.9	5719.3	6638.0	5331.6	5892.3	6804.0	5452.7	6031.8	6993.7
9	5291.6	5844.1	6731.8	5390.4	5953.7	6860.6	5605.8	6192.9	7142.3
10	5540.3	6120.0	7053.5	5547.6	6090.5	7100.2	5752.3	6311.1	7268.0

Let us consider a square FGM plate with the parameters mentioned in Section 3.1, but the plate is clamped at its four edges. The natural frequencies of the fully clamped FGM plate with a central hole 0.2, 0.3, or 0.4 m in diameter for different values of the exponent n are listed in Table 2. The natural frequencies increase with increasing hole diameter for $n \leqslant 5$ as well, which is a result of reduction in the volume fraction of the metallic phase.

CONCLUSIONS

The static and free vibration analyses of an FGM plate with a circular hole are performed on the basis of the three-dimensional theory of elasticity. The material properties vary continuously over the plate thickness. The graded finite element method and the Rayleigh–Ritz energy formulation are applied. Comparisons with available results show good agreement. Effects of the volume fractions of the ceramic and metallic phases on the static behavior of FGM plates under uniaxial tension and on the natural frequencies of a fully clamped plate are investigated. The results obtained in the present study show that the mechanical stress distribution and natural frequencies can be modified to desired ones by selecting appropriate volume fractions of the constituent materials. In particular, the stress field around the circular cutout in the FGM plate can be effectively reduced. The use of graded elements provides smoother and more accurate results than homogeneous elements.

REFERENCES

1. S. Suresh and A. Mortensen, *Fundamentals of Functionally Graded Materials* (IOM Comm., London, 1998).
2. J. N. Reddy and Z. Q. Cheng, "Three Dimensional Thermomechanical Deformations of Functionally Graded Rectangular Plates," Europ. J. Mech. A. Solids **20**, 841–855 (2001).
3. S. S. Vel and R. C. Batra, "Exact Solution for Thermoelastic Deformations of Functionally Graded Thick Rectangular Plates," AIAA J. **40** (7), 1421–1433 (2002).
4. M. Kashtalyan, "Three-Dimensional Elasticity Solution for Bending of Functionally Graded Plates," Europ. J. Mech. A. Solids **23**, 853–864 (2004).
5. C. F. Lu, C. W. Lim, and W. Q. Chen, "Semi-Analytical Analysis for Multi-Directional Functionally Graded Plates: 3-D Elasticity Solutions," Int. J. Numer. Methods Eng. **79**, 25–44 (2009).

6. P. H. Wen, J. Sladek, and V. Sladek, "Three-Dimensional Analysis of Functionally Graded Plates," Int. J. Numer. Methods Eng. **87** (10), 923–942 (2011).
7. J. N. Reddy and C. D. Chin, "Thermomechanical Analysis of Functionally Graded Cylinders and Plates," J. Thermal Stresses **26** (1), 593–626 (1998).
8. J. N. Reddy, "Analysis of Functionally Graded Plates," Int. J. Numer. Methods Eng. **47**, 663–684 (2000).
9. L. D. Croce and P. Venini, "Finite Elements for Functionally Graded Reissner–Mindlin Plates," Comput. Methods Appl. Mech. Eng. **193**, 705–725 (2004).
10. I. Mechab, H. A. Atmane, A. Tounsi, et al., "A Two Variable Refined Plate Theory for the Bending Analysis of Functionally Graded Plates," Acta Mech. Sinica **26**, 941–949 (2010).
11. T. Prakash and M. Ganapathi, "Asymmetric Flexural Vibration and Thermoelastic Stability of FGM Circular Plates Using Finite Element Method," Composites. Pt B **37**, 642–649 (2006).
12. S. H. Chi and Y. L. Chung, "Mechanical Behavior of Functionally Graded Material Plates under Transverse Load. Pt 1. Analysis," Int. J. Solids Structures **43**, 3657–3674 (2006).
13. H. Matsunaga, "Free Vibration and Stability of Functionally Graded Plates According to a 2-D Higher-Order Deformation Theory," Composite Structures **82**, 499–512 (2008).
14. E. Orakdogen, S. Kucukarslan, A. Sofiyev, and M. H. Omurtag, "Finite Element Analysis of Functionally Graded Plates for Coupling Effect of Extension and Bending," Meccanica **45**, 63–72 (2010).
15. M. K. Singha, T. Prakash, and M. Ganapathi, "Analysis of Functionally Graded Plates Using an Edge-Based Smoothed Finite Element Method," Finite Elements Anal. Design. **47**, 453–460 (2011).
16. H. Nguyen-Xuan, L. V. Tran, C. H. Thai, and T. Nguyen-Thoi, "Analysis of Functionally Graded Plates by an Efficient Finite Element Method with Node-Based Strain Smoothing," Thin-Walled Structures **54**, 1–18 (2012).
17. M. H. Santare and J. Lambros, "Use of Graded Finite Elements to Model the Behavior of Nonhomogeneous Materials," J. Appl. Mech. **67**, 819–822 (2000).
18. J.-H. Kim and G. H. Paulino, "Isoparametric Graded Finite Elements for Nonhomogeneous Isotropic and Orthotropic Materials," J. Appl. Mech. **69**, 502–514 (2002).
19. Z. Zhang and G. H. Paulino, "Wave Propagation and Dynamic Analysis of Smoothly Graded Heterogeneous Continua Using Graded Finite Elements," Int. J. Solids Structures **44**, 3601–3626 (2007).
20. M. H. Santare, P. Thamburaj, and G. A. Gazonas, "The Use of Graded Finite Elements in the Study of Elastic Wave Propagation in Continuously Nonhomogeneous Materials," Int. J. Solids Structures **40**, 5621–5634 (2003).
21. E. V. Dave, G. H. Paulino, and W. G. Buttlar, "Viscoelastic Functionally Graded Finite Element Method Using Correspondence Principle," J. Mater. Civil Eng. **23**, 39–48 (2011).
22. M. Asgari, M. Akhlaghi, and S. M. Hosseini, "Dynamic Analysis of Two-Dimensional Functionally Graded Thick Hollow Cylinder with Finite Length under Impact Loading," Acta Mech. **208**, 163–180 (2009).
23. M. Asgari and M. Akhlaghi, "Natural Frequency Analysis of 2D-FGM Thick Hollow Cylinder Based on Three-Dimensional Elasticity Equations," Europ. J. Mech. A. Solids **30**, 72–81 (2011).
24. K. Asemi, M. Salehi, and M. Akhlaghi, "Elastic Solution of a Two-Dimensional Functionally Graded Thick Truncated Cone with Finite Length under Hydrostatic Combined Loads," Acta Mech. **217**, 119–134 (2011).
25. L.-L. Cao, Q.-H. Qin, and N. Zhao, "Hybrid Graded Element Model for Transient Heat Conduction in Functionally Graded Materials," Acta Mech. Sinica **28**, 128–139 (2012).
26. K. Asemi, M. Akhlaghi, and M. Salehi, "Dynamic Analysis of Thick Short FGM Cylinders," Meccanica **47**, 1441–1453 (2012).
27. T. K. Paul and K. M. Rao, "Finite-Element Stress-Analysis of Laminated Composite Plates Containing 2 Circular Holes under Transverse Loading," Comput. Structures **54** (4), 671–677 (1995).
28. R. T. Tenchev, M. K. Nygard, and A. Echtermeyer, "Design Procedure for Reducing the Stress-Concentration around Circular Heres in Laminated Composites," Composites **26** (12), 815–828 (1995).
29. M. Y. Kaltakci, "Stress Concentrations and Failure Criteria in Anisotropic Plates with Circular Holes Subjected to Tension or Compression," Comput. Structures **61** (1), 67–78 (1996).
30. A. Haque, L. Ahmed, and A. Ramasetty, "Stress Concentrations and Notch Sensitivity in Woven Ceramic Matrix Composites Containing a Circular Hole—An Experimental, Analytical, and Finite Element Study," J. Amer. Ceramic Soc. **88** (8), 2195–2201 (2005).
31. D. V. Kubair and B. Bhanu-Chandar, "Stress Concentration Factor due to a Circular Hole in Functionally Graded Panels under Uniaxial Tension," Int. J. Mech. Sci. **50**, 732–742 (2008).
32. M. Mohammadi, J. R. Dryden, and L. Jiang, "Stress Concentration Around a Hole in a Radially Inhomogeneous Plate," Int. J. Solids Structures **48**, 483–491 (2011).

33. C. Hu, X.-Q. Fang, and W.-H. Huang, "Multiple Scattering of Shear Waves and Dynamic Stress from a Circular Cavity Buried in a Semi-Infinite Slab of Functionally Graded Materials," Eng. Fracture Mech. **75**, 1171–1183 (2008).
34. X. Q. Fang, C. Hu, and S. Y. Du, "Strain Energy Density of a Circular Cavity Buried in Semi-Infinite Functionally Graded Materials Subjected to Shear Waves," Theoret. Appl. Fracture Mech. **46**, 166–174 (2006).
35. S. K. Deb Nath, C. H. Wong, and S.-G. Kim, "A Finite-Difference Solution of Boron/Epoxy Composite Plate with an Internal Hole Subjected to Uniform Tension/Displacements Using Displacement Potential Approach," Int. J. Mech. Sci. **58**, 1–12 (2012).
36. M. Janghorban and A. Zare, "Thermal Effect on Free Vibration Analysis of Functionally Graded Arbitrary Straight-Sided Plates with Different Cutouts," Latin Amer. J. Solids Structures **8**, 245–257 (2011).
37. Q. Yang, C.-F. Gao, and W. Chen, "Stress Analysis of a Functional Graded Material Plate with a Circular Hole," Arch. Appl. Mech. **80**, 895–907 (2010).
38. A. Linkov and L. Rybarska-Rusinek, "Evaluation of Stress Concentration in Multi-Wedge Systems with Functionally Graded Wedges," Int. J. Eng. Sci. **61**, 87–93 (2012). DOI: 10.1016/ j.ijengsci.2012.06.012.
39. S. Timoshenko and J. N. Goodier, *Theory of Elasticity* (McGraw-Hill, New York, 1970).
40. O. C. Zienkiewicz and R. L. Taylor, *The Finite Element Method for Solid and Structural Mechanics* (Elsevier, Oxford, 2005).
41. R. D. Cook, D. S. Malkus, M. E. Plesha, and R. J. Witt, *Concepts and Applications of Finite Element Analysis* (John Wiley and Sons, New York, 2001).
42. A. Rezaei Mojdehi, A. Darvizeh, A. Basti, and H. Rajabi, "Three-Dimensional Static and Dynamic Analysis of Thick Functionally Graded Plates by the Meshless Local Petrov–Galerkin (MLPG) Method," Eng. Anal. Boundary Elements **35**, 1168–1180 (2011).
43. Z. Yang, C. B. Kim, C. Cho, and H. G. Beom, "The Concentration of Stress and Strain in Finite Thickness Elastic Plate Containing a Circular Hole," Int. J. Solids Structures **45**, 713–731 (2008).
44. A. J. M. Ferreira, R. C. Batra, C. M. C. Roque, et al., "Natural Frequencies of Functionally Graded Plates by a Meshless Method," Composite Structures **75**, 593–600 (2006).